Holzforschung, Vol. 60, pp. xxx-xxx, 2006 • Copyright © by Walter de Gruyter • Berlin • New York. DOI 10.1515/HF.2006.XXX

Spatial relationships between polymers in Sitka spruce: Proton spin-diffusion studies

Clemens Altaner[1], David C. Apperley[2] and Michael C. Jarvis[1,*]

[1] Chemistry Department, University of Glasgow, Glasgow, UK

[2] Chemistry Department, University of Durham, Durham, UK

*Corresponding author.
Chemistry Department, Glasgow University, Glasgow G12 8QQ, UK
E-mail: mikej@chem.gla.ac.uk

Abstract

The spatial arrangement of polymers in Sitka spruce (*Picea sitchensis*) was investigated by NMR proton spin-diffusion studies, supplemented by deuterium-exchange experiments monitored by FTIR spectroscopy. The FTIR spectra of earlywood sections after vapour-phase exchange with deuterium oxide showed that 43% of the hydroxyl groups were accessible to deuteration. This value is lower than predicted in the absence of aggregation of cellulose microfibrils into larger units, but greater than the predicted level of deuteration if 3.5-nm microfibrils surrounded by hemicellulose sheaths were aggregated into 4×4 arrays without space for deuterium oxide to penetrate between the microfibrils. The rate of proton spin diffusion between lignin and cellulose was consistent with the presence of microfibril arrays with approximately these dimensions and with lignin located outside them, in both earlywood and latewood. Proton spin-diffusion data for hemicelluloses were complicated by difficulties in assigning signals to glucomannans and xylans, but there was evidence for the spatial association of one group of hemicelluloses, including acetylated glucomannans, with cellulose surfaces, while another group of hemicelluloses was in spatial proximity to lignin. These data are consistent with a number of nanoscale models for the Sitka spruce cell wall, including a model in which glucomannans are associated with microfibril surfaces within the aggregate and water can penetrate partially between these surfaces, and one in which all non-cellulosic polymers and water are excluded from the interior of each microfibril aggregate.

Keywords: cell wall models; cellulose; hemicellulose; lignin; NMR spectroscopy; supramolecular structure of wood.

Introduction

The diffusion of nuclear magnetisation (nuclear spin order) through solids can be used in NMR experiments to estimate domain sizes, for example the dimensions of the components of a composite material (Zhang and Mehring 1989). Wood is well suited to this approach because it gives ^{13}C solid-state NMR spectra that are rich in structural information (Haw et al. 1984; Newman and Hemmingson 1990; Hult et al. 2000; Maunu 2002).

Bardet et al. (1986) were able to obtain spatial information on wood polymers from ^{13}C spin diffusion experiments, but this approach is only practical if ^{13}C-enriched wood is available. However proton spin-diffusion experiments can be carried out without isotopic enrichment. Newman (1992) used a modification of the Goldman-Shen proton spin-diffusion experiment with detection using the ^{13}C spectrum (Zhang and Mehring 1989) to examine spatial relationships in softwood and hardwood cell walls.

It is possible to deduce more limited spatial information from simpler NMR experiments in which the proton relaxation-time constants for different polymers are observed to be averaged by spin diffusion during the relaxation period. In the cell walls of dry hardwood (Tekely and Vignon 1987a) and softwood (Haw et al. 1984), proton spin equilibration during periods of the order of 10 ms averaged the rotating-frame spin-lattice relaxation time ^1H $T_{1\rho}$ for signals assigned to lignin and crystalline cellulose, implying a spatial proximity for these polymers. However, distinct values of ^1H $T_{1\rho}$ were observed in water-saturated wood by Newman (1992), Ahvazi and Argyropoulos (1999) and Liitia et al. (2000). The swelling of the wood structure on hydration may contribute to this isolation of the lignin and cellulose proton spin systems from one another, but another contributing factor is that the proton spin-diffusion coefficient D is decreased by the greater thermal mobility of hydrated wood polymers. The value of D may be calculated from:

$$D = 0.13d^2/T_2, \quad (1)$$

where the constant d is approximately 0.26 nm for cellulose (Newman 1992). The proton spin-spin relaxation time T_2 is measurable in NMR experiments (Tekely and Vignon 1987b) and increases with thermal mobility. Values of the proton spin-diffusion coefficient D of the order of 1 $nm^2\ ms^{-1}$ calculated in this way are typical for crystalline polysaccharides.

The detailed spin-diffusion experiments of Newman (1992) on *Pinus radiata* are of topical interest because they suggested that cellulose fibrils of approximately 14 nm wide, much greater than the lateral dimensions of a single cellulose microfibril, were embedded in a matrix containing lignin. Recent evidence from atomic force microscopy and other techniques (Singh et al. 2002; Terashima et al. 2004; Fahlén and Salmén 2005) suggests that in the S2 layer of softwood cell walls, cellulose microfibrils are aggregated into bundles that are

10–20 nm thick, with at least some of the lignin and hemicellulosic glucomannans or xylans located between these. Drying opens radial and tangential cracks between these aggregates of microfibrils (Singh et al. 2002). Detailed knowledge of the way in which non-cellulosic polymers are distributed through this system will be essential if we are to reach an understanding of how softwood cell walls absorb water and how they deform at the nanometre scale under mechanical stress.

In the research described here we revisited the proton spin-diffusion experiment of Newman (1992). We have taken advantage of modern developments in the detailed design of the pulse sequences used, but we retained the basic mixing of proton spins (MOPS) format of the Newman (1992) experiment. The sample, containing approximately the saturation content of water, is first uniformly magnetised at the proton resonance frequency. The proton magnetisation is then allowed to decay to different extents in spatial domains where the polymers differ in thermal mobility. The system re-equilibrates by proton spin-diffusion and exchange reactions, and the evolution of proton magnetisation in each polymer is followed by cross-polarisation to ^{13}C and monitoring the peak intensities corresponding to individual polymers in the ^{13}C NMR spectrum.

Newman (1992) used rotating-frame spin-lattice (^1H $T_{1\rho}$) relaxation to induce the initial imbalance in proton magnetisation. When ^1H $T_{1\rho}$ relaxation is adopted, magnetisation of thermally mobile polymers in close contact with water is selectively depleted. In the subsequent step, proton spin diffusion from the rigid, cellulosic core of the microfibrils, down the magnetisation gradient to the mobile, hydrated outer layers re-equilibrates the proton magnetisation throughout the system. Newman (1992) pointed out that the spin diffusion processes observed in this experiment are those with time constants that lie between ^1H $T_{1\rho}$, which sets up the initial magnetisation gradient, and ^1H T_1, which dissipates proton magnetisation universally. One problem is that spin diffusion over short distances of 1–2 nm, for example, within cellulose crystallites that are ca. 3 nm wide, is too fast to be observed in this way.

A different form of this experiment making use of spin-spin (^1H T_2) relaxation (Zhang and Mehring 1989) has been applied to primary cell walls from non-woody plants (Ha et al. 1998). When ^1H T_2 relaxation is used, it is the magnetisation of the rigid polymers that is selectively depleted and the magnetisation gradient is inward towards the centre of the microfibrils. One advantage is that for relatively rigid solids such as wood, ^1H T_2 relaxation is much faster than ^1H $T_{1\rho}$ relaxation, so that ^1H spin diffusion over shorter paths, and thus on shorter timescales, can be observed. Ha et al. (1998) were able to detect spin diffusion between the surface and interior chains of primary-wall cellulose, although they could not calculate absolute radial diffusion distances using Eq. (1) because spin diffusion was apparently anisotropic.

We applied ^1H T_2-based pulse sequences of this type to hydrated Sitka spruce, accompanied by deuterium-exchange FTIR measurements of the degree of hydration and by modelling of hydration and proton spin diffusion.

Material and methods

Sample preparation

The wood used was from the 13th to 15th annual rings at the stem base of a Sitka spruce [*Picea sitchensis* (Bong.) Carrière] tree grown at Kershope, Northumbria, UK and felled at 36 years of age. Latewood was excised with a fine-toothed scroll saw and split into sticks of approximately 1 mm square. Earlywood was compressed in a hydraulic press to approximately three times its initial density to allow the maximum mass to be packed into the NMR rotor, and was split as for latewood. The wood was soaked overnight to absorb approximately 0.5 $cm^3\ g^{-1}$ H_2O.

NMR spectroscopy

Spectra were obtained on a Varian Unity Inova spectrometer operating at 75.430 MHz for ^{13}C. Effective proton spin-spin relaxation times ^1H T_2 were measured using a pulse sequence that incorporated a spin-echo (90-τ-180-τ) with variable delay time τ on the ^1H channel, followed by a cross-polarisation step with fixed, matched radiofrequency fields of 56 kHz on both channels. Spectra were acquired with a contact time of 0.2 ms, recycle delay of 1 s, spin rate of 5 kHz and ^1H decoupling field of 75 kHz.

The pulse sequence for the proton spin-diffusion experiments incorporated a spin-echo (90-τ-180-τ) with 15-μs delay time τ on the ^1H channel, followed by a z-filter consisting of two 90° pulses with alternating phase separated by a mixing time T_m (Zhang and Mehring 1989). A cross-polarisation period followed the second 90° pulse. This consisted of a fixed 56-kHz radiofrequency field on the ^{13}C channel and a linearly amplitude-ramped (56 to 42 kHz in 20 steps) spin-lock pulse on the ^1H channel. Spectra were acquired as a function of the mixing time at a spin rate of 6 kHz, contact time of 0.5 ms, recycle delay of 1 s and with a ^1H decoupling field of 85 kHz.

Modelling of spin diffusion

The diagrammatic cross-sectional model of a structural unit of the spruce cell wall shown in Figure 1 was constructed on a 0.6-nm square grid, approximately the cross-sectional area of one polysaccharide chain in the dry state. Each cell on the grid was assigned a relative proton magnetisation at the start of the spin-diffusion period, a value for the spin-lattice relaxation constant ^1H T_1 and a local value of the proton spin-diffusion coefficient. The relative proton magnetisation in each cell was allowed to evolve through magnetisation transfer across cell boundaries in steps of 1 ms. Spin diffusion across the outer boundaries of the grid was disallowed, a condition equivalent to assuming that the structural unit defined by the grid repeats infinitely.

FTIR microscopy

Radial-longitudinal sections of 10–20 mm in thickness were equilibrated with dry nitrogen or nitrogen saturated with D_2O in a through-flow cell with barium fluoride top and bottom windows. FTIR spectra were obtained from 150×50-μm^2 areas apertured within the microscope field of a Nicolet Continuum FTIR microscope interfaced to a Nicolet Nexus spectrometer. The spectral resolution was 4 cm^{-1} and 64 scans were averaged for each spectrum, with approximately six independent spectra averaged. In these experiments it was essential to be able to dry the wood sections completely without exchange with atmospheric nitrogen. This was accomplished by a gas-flow control system allowing switching between dry and D_2O-saturated nitrogen without exposure to air. To prevent back-diffusion of external air, the outflow from the cell was extended with tubing dipping

into a D_2O reservoir. The inflow nitrogen was dried through successive columns of aluminosilicate drying agent and powdered phosphorus pentoxide. In spectra of dried or deuterated sections, the total intensity of the hydroxyl stretching region was stable for up to 1 h, indicating equilibration with D_2O and the absence of H_2O contamination over this time, which considerably exceeded the duration of the measurements.

Results

FTIR microspectroscopy: accessibility to deuteration

Because the rigidity and NMR relaxation characteristics of each wood polymer depend on hydration, it was necessary to establish whether water was able to penetrate throughout the structure or whether, for example, the surfaces of cellulose microfibrils became inaccessible to water when they aggregated together (Larsson et al. 1997). This question was addressed by deuterium-exchange FTIR microscopy.

Longitudinal sections of Sitka spruce earlywood were dehydrated in extremely dry nitrogen until the FTIR microspectra showed no further decrease in the intensity of the hydroxyl stretching bands (3200–3600 cm^{-1}) predominately due to cellulose and hemicelluloses. The sections were then deuterated by vapour-phase exchange and dried again, which shifted the stretching bands of the exchangeable hydroxyl groups to 2400–2600 cm^{-1} (Figure 2). The percentage of exchangeable hydroxyls throughout the early wood cell wall was 43.4% with SD 5.7% (n = 8).

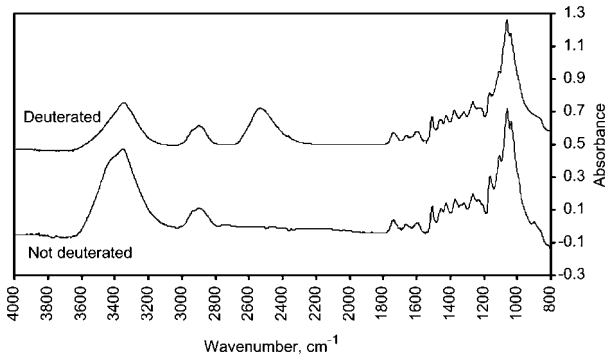

Figure 2 Transmission FTIR spectra of dry Sitka spruce earlywood with and without deuterium exchange. The broad peak at 3100–3600 cm^{-1} corresponds to stretching vibrations of hydroxyl groups. Deuteration of hydroxyl groups accessible to water removed their contribution to the total O–H stretching intensity to the O–D stretching frequency of 2400–2600 cm^{-1}. The spectra shown are each averaged from eight measurement fields after normalisation according to the C–H stretching band intensity (2800–3000 cm^{-1}), which is unaffected by deuterium exchange.

NMR spectra and proton spin-spin relaxation

Standard CP-MAS ^{13}C NMR spectra of hydrated earlywood and latewood of Sitka spruce are shown in Figure 3. The earlywood and latewood spectra are closely similar and are typical of softwoods (Kim and Newman 1995; Ahvazi and Argyropoulos 1999; Hult et al. 2000; Liitia et al. 2000; Sivonen et al. 2003; Wikberg and Maunu 2004). Spectral assignments are shown in Table 1. Problems in

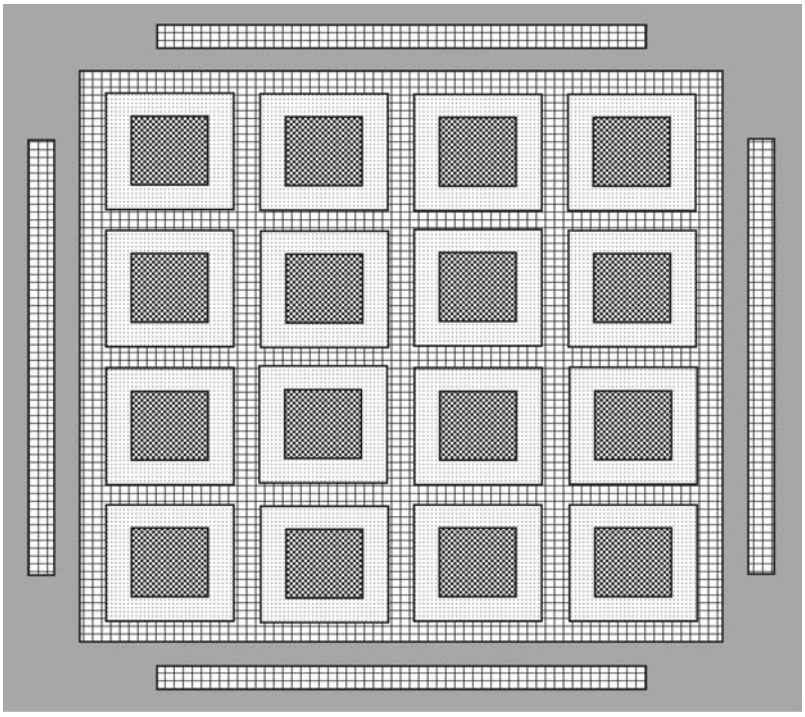

Figure 1 Simplified model of a polymer aggregate comprising one unit of a Sitka spruce cell wall, reduced to a grid of 0.6 nm × 0.6 nm squares. A 4 × 4 array of cellulose microfibrils, each with a cellulose I core and a distinct monolayer of surface chains, is embedded in sheathing hemicelluloses and surrounded by a matrix containing lignin and matrix hemicelluloses.

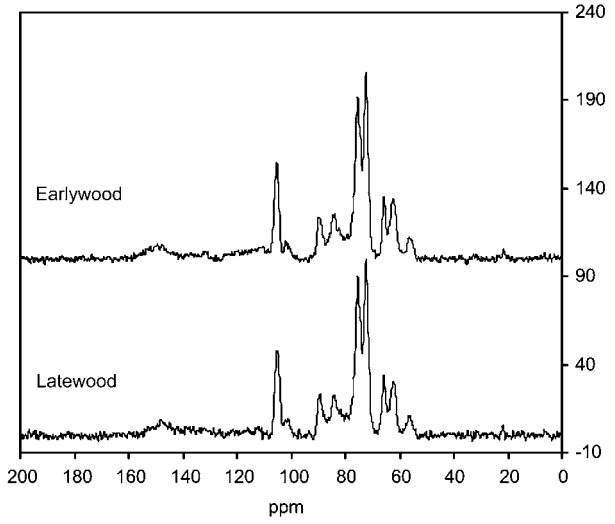

Figure 3 CP-MAS solid-state ^{13}C NMR spectra of hydrated earlywood and latewood from Sitka spruce. For peak assignments see Table 1.

the assignment of hemicellulose signals are dealt with in the Discussion section.

The first step in the spin-diffusion experiment is to set up proton magnetisation gradients through selective relaxation. Since the proton spin-spin relaxation process has not been widely studied in wood (Tekely and Vignon 1987b), a preliminary spin-spin relaxation study on hydrated earlywood and latewood of Sitka spruce was conducted.

Figure 4 shows proton spin-spin relaxation curves for the principal peaks in the ^{13}C spectra of early wood. The polysaccharides behaved as rigid solids, with fitted values of the effective ^1H T_2 less than 10 μs for all ^{13}C peaks assigned to cellulose, and just over 10 μs for hemicellulosic peaks. Peaks assigned to lignin gave consistently longer effective values of ^1H T_2. The least-squares fitting was based on a Gaussian model, which is appropriate for materials of the rigidity observed for the polysaccharides. A transition to Lorentzian behaviour may be encountered in the ^1H T_2 relaxation of more mobile materials (Ha et al. 1996), but the signal/noise ratio of the lignin peaks was insufficient to distinguish between Lorentzian and Gaussian models.

Proton spin diffusion

It was necessary to begin the ^1H spin-diffusion after a spin-echo delay of 15 μs to obtain sufficient discrimination between rigid and more mobile polymers through differences in ^1H T_2. This delay time reduced the signal intensities to between 4% (cellulose) and 15% (lignin) of the original intensity. After a delay of 15 μs, it may be assumed that proton magnetisation in free water remained close to its original value, and thus at the end of the delay time, water protons would have retained the majority of the total proton magnetisation present in the whole sample. The substantial loss in intensity of the polysaccharide signals made it more difficult to elucidate the spin-diffusion characteristics of the smaller peaks in the ^{13}C spectrum. In the case of lignin the inefficiency of cross-polarisation led to a further signal loss for aromatic carbon nuclei, even at zero spin-echo delay, and therefore only the methoxyl signal was used to probe the behaviour of the lignin component.

Table 1 Signal assignments for ^{13}C NMR spectra of Sitka spruce.

Signal (ppm)	Assignment	Location
147	Lignin, guiacyl units	C-3
133	Lignin, guiacyl units	C-1
105	Cellulose	C-1
102	Hemicellulose	C-1
89	Cellulose Iα and Iβ	C-4
84	Cellulose, surface chains	C-4
82	Hemicelluloses	C-4
80	Hemicelluloses	C-4
75	Cellulose, hemicelluloses	C-2,C-3
72	Cellulose, hemicelluloses	C-3, C-5
65	Cellulose Iα and Iβ	C-6
62	Cellulose, hemicelluloses	C-6
56	Lignin	O–CH_3
21	Acetyl	CH_3

A problem in the design of proton spin-diffusion experiments is that laboratory-frame spin-lattice (^1H T_1) relaxation results in the decay of all signals during the mixing time, which is faster for the more mobile polymers in the system. Zhang and Mehring (1989) introduced some of the features of the inversion-recovery experiment commonly used to measure ^1H T_1 to alleviate the ensuing problems in interpreting spin-diffusion data. This procedure was followed by Newman (1992) and by us. Kenwright and Packer (1990) pointed out that it does not fully account for ^1H T_1 effects and suggested that further measures are necessary before these effects can be eliminated. Here we incorporated variation in ^1H T_1 into the modelling of signal evolution with mixing time (see below).

Figure 5 shows how the conventional and inverted signal intensity, integrated across the whole spectral range,

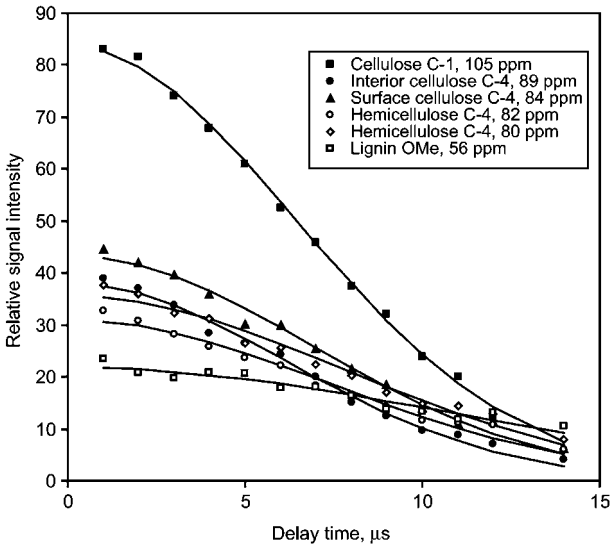

Figure 4 Proton spin-spin relaxation (^1H T_2) curves for selected peaks in the ^{13}C NMR spectrum of Sitka spruce latewood. Solid lines are based on least-squares fitting of Gaussian decay curves.

evolved through ^{1}H T_1 relaxation and spin diffusion. The positive and negative curves correspond to proton magnetisation evolving in the +Z and -Z directions, respectively, so that the amplitude $A(T_m)$ between the two curves at any mixing time T_m is two-fold the net magnetisation in either direction, cancelling out much of the contribution from ^{1}H T_1 decay and imperfections in the initial 90° pulse (Zhang and Mehring 1989). In our experiments $A(T_m)$ increased up to $T_m = 100$ ms due to the diffusion of proton magnetisation from water molecules, which are not represented in the ^{13}C spectrum. Spectral variation in $A(T_m)$ describes the redistribution of proton magnetisation by spin diffusion amongst components of varying mobility.

Individual signals were normalised against the total signal intensity $A(T_m)$ at each value of the mixing time T_m. The evolving signal intensities for large and small peaks in the ^{13}C spectrum were still difficult to compare visually, so an additional normalisation step was introduced. The resulting normalised signal intensities remained essentially constant for each peak after a mixing time of 25.6 ms, as observed by Newman (1992), because the redistribution of ^{1}H magnetisation by spin diffusion was essentially complete by that time. Therefore, the second normalisation step was based on the relative signal intensity averaged over only those mixing times between 25.6 and 205 ms. This normalisation procedure is different from that used by Newman (1992). It makes the redistribution of ^{1}H magnetisation amongst different polymers easier to visualise by removing the effect of simultaneous ^{1}H T_1 decay. The convergence of the upper and lower curves at long mixing times (Figure 5) is consistent with an overall value of approximately 1 s for ^{1}H T_1. Only slight spectral variation in ^{1}H T_1 relaxation was detectable due to the averaging effect of spin diffusion (data not shown) and detailed modelling of the evolution of signal intensity would have been required to extract the observed ^{1}H T_1 time constant at each point in the spectrum. This was not attempted owing to the complexity of the early part of the signal intensity curves.

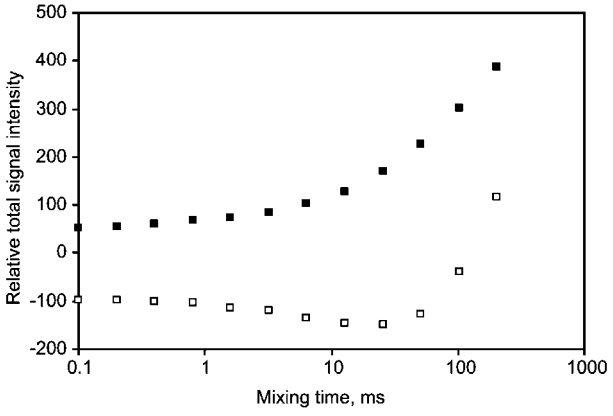

Figure 5 Evolution of total signal intensity, summed across all peaks in the ^{13}C NMR spectra of Sitka spruce earlywood, as a function of the mixing time T_m in a proton spin-diffusion experiment. The alternating phase of the final proton 90° pulse led to separate positive (closed squares) and negative (open squares) signal intensities at short mixing times. The amplitude between the positive and negative signal intensity curves is a measure of net proton magnetisation at a given mixing time T_m and decreased at long mixing times due to ^{1}H T_1 relaxation. The increase in amplitude at shorter mixing times was due to transmission of proton magnetisation from water, which is not represented in the ^{13}C NMR spectrum.

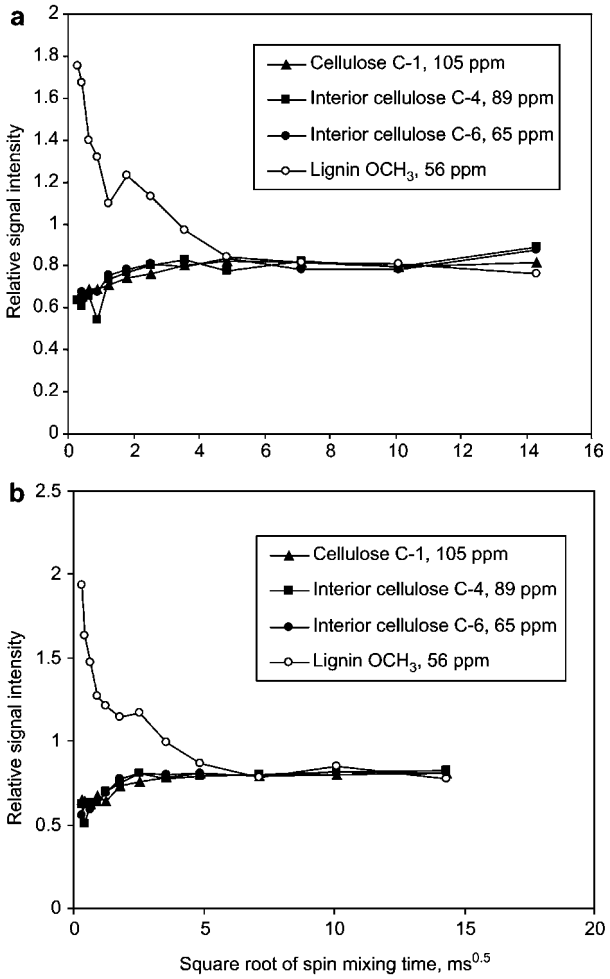

Figure 6 Normalised proton spin equilibration curves for cellulose and lignin peaks in the ^{13}C spectra of Sitka spruce latewood (above) and earlywood (below). Normalised signal intensity is plotted against the square root of the mixing time T_m, which is a measure of the distance over which spin diffusion is required to equilibrate signals from two polymers, with the approximation that the spin diffusion coefficient is assumed to be constant.

The spin mixing curves (Figures 6–8) show how the relative ^{1}H magnetisation associated with each peak in the ^{13}C spectrum equilibrated through spin diffusion. Figure 6 shows that proton magnetisation in lignin equilibrated completely with proton magnetisation in cellulose within a mixing time of 20–30 ms. This is in close agreement with the observations of Newman (1992), despite the differences in experimental procedure.

Figure 7 shows the proton spin mixing between cellulosic and hemicellulosic chains, as indicated by their C-4 signals. The relative intensity of the C-4 signals at 89 and 84 ppm, corresponding to ordered and less ordered cellulose domains, respectively, is widely used as a measure of crystallinity (Newman and Hemmingson 1990). Spin equilibration between these two signals was clearly evident and was complete within a mixing time of 5–10 ms. This may be a slight overestimate of the mixing

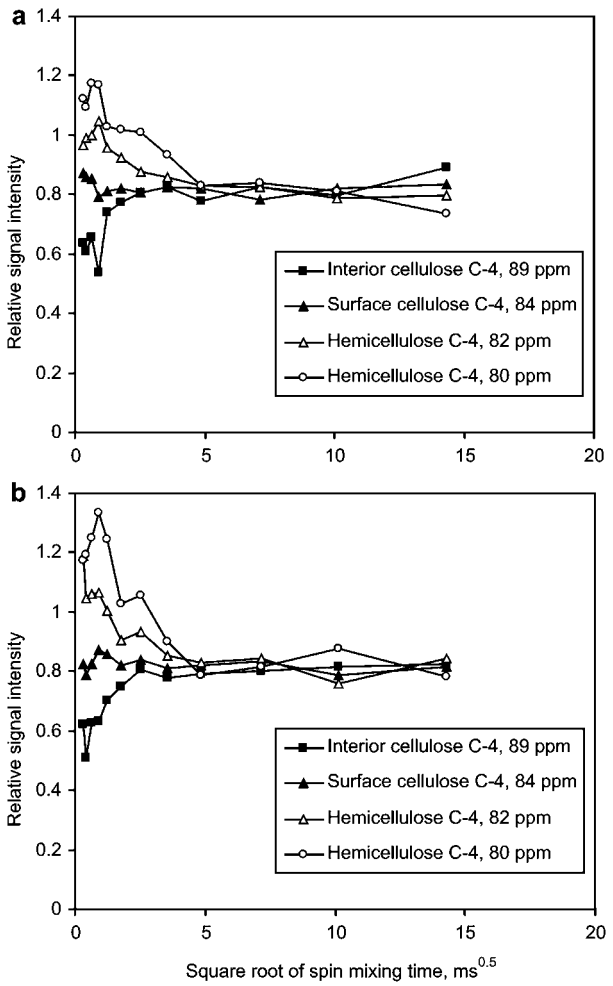

Figure 7 Normalised proton spin equilibration curves for C-4 peaks from cellulose and hemicelluloses in the ^{13}C spectra of Sitka spruce latewood (above) and earlywood (below).

time required if xylans make a significant contribution to the 84-ppm signal (Teleman et al. 2001). We assume that most of the cellulose contributing to the signal intensity around 84 ppm was located at the microfibril surfaces (Wickholm et al. 1998; Newman 1999). The rapid equilibration between the groups of signals at 84 and 89 ppm is consistent with this assumption.

The hemicellulosic C-4 signals at 80–82 ppm were heterogeneous in their behaviour and were divided arbitrarily into two parts (Figure 7). Higher initial magnetisation indicated greater thermal mobility than for cellulose. The hemicellulosic C-4 signal, particularly the part centred on 80 ppm, showed a rapid increase in the first 1 ms of spin mixing. This suggests spin diffusion from an adjacent, more mobile component, which could be acetyl substituents on the hemicellulose itself or lignin molecules in close proximity. A simultaneous rapid drop in proton magnetisation of both lignin (Figure 6) and acetyl (Figure 8) is consistent with this interpretation. At longer mixing times the equilibration curves followed by the lignin methoxyl and hemicellulose C-4 signals were very similar, differing considerably from that of the acetyl signal. This observation implies that lignin was the source of at least part of the proton magnetisation that diffused rapidly to those hemicelluloses with a C-4 signal at 80 ppm. The acetyl signal appeared to converge with the 82-ppm hemicellulose C-4 signal after less than 10 ms of mixing time, suggesting that polymers associated with this signal were acetylated.

The hemicellulosic C-1 signal centred on 101 ppm was of low intensity, accounting for only 20% of the total C-1 signal. This gave rise to considerable scatter in its intensity, but it appeared to equilibrate with the cellulose C-1 signals after approximately 20 ms of mixing time (Figure 8). To investigate whether the remainder of the hemicellulosic C-1 signals were obscured by the large cellulose C-1 signal at 105 ppm, the latter was divided into three bands, each 1 ppm wide, centred on 104, 105 and 106 ppm. The upfield wing (104 ppm) of the cellulose C-1 peak showed slightly greater initial mobility than the rest, equilibrating after approximately 10 ms. Since the 104- and 106-ppm signals are both normally assigned to cellulose Iβ, there is no reason to expect them to differ in location or mobility, and it is more likely that the 104-ppm signal contains a contribution from hemicelluloses.

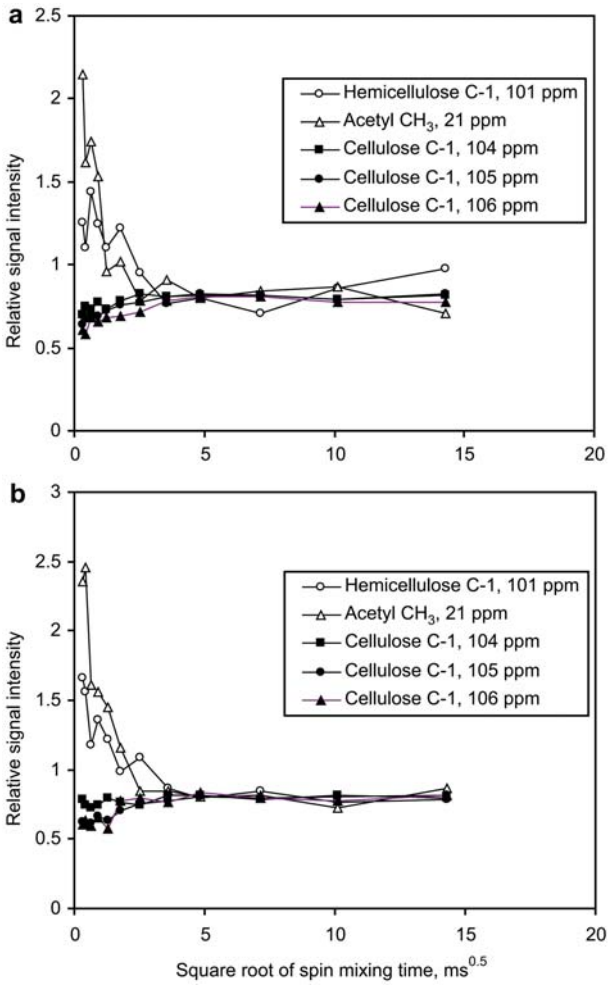

Figure 8 Normalised proton spin equilibration curves for the C-1 peak from hemicelluloses, the CH_3 peak from acetyl groups, and various regions of the C-1 peak from cellulose in the ^{13}C spectra of Sitka spruce latewood (above) and earlywood (below).

Discussion and conclusion

The minor differences between latewood (LW) and earlywood (EW) are likely due to greater water retention in the latter during magic-angle spinning rather than to any structural differences. Thus, the NMR features of EW and LW can be interpreted together. The FTIR study was restricted to EW, because LW cell walls are too thick to obtain high-quality FTIR spectra in transmission.

The extent of deuteration observed by FTIR (43.4 ± 5.7%) was compared with three sets of predictions based on the microfibril aggregates proposed by Fahlén and Salmén (2005) (Figure 1) and the composition data of Bertaud and Holmbom (2004), but with different assumptions about the locations accessible to water. In all three models it is assumed that the core chains of each microfibril, below the surface monolayer, are inaccessible to deuteration. For simplicity we neglected the possibility that disordered regions, accessible to internal deuteration, were interspersed along the microfibrils. This simplification does not affect the model predictions, because the proportion of chains assigned to the surface was originally calculated from the NMR signal intensity in the 82–86-ppm region, which would include any such disordered chain segments.

In model 1, cellulose surfaces within aggregates and a subset of hemicelluloses associated with these were considered to be inaccessible to deuteration. The predicted deuteration for model 1 was 32.3%, which was significantly less than observed. In model 2, cellulose surfaces within aggregates were considered to be inaccessible, but all hemicelluloses were accessible, either because some D_2O penetrated between microfibrils within an aggregate or because all the hemicelluloses were located outside the aggregates. The predicted deuteration for model 2 was 40.0%, which is comparable within experimental error to the extent of deuteration observed. In model 3, all cellulose surfaces and all hemicellulose were accessible to deuteration. This would require that aggregation was absent or that D_2O was able to penetrate between all the microfibrils within an aggregate. The predicted deuteration for model 3 was 73.3%, significantly greater than the level observed. Model 2, or something similar, is implicitly suggested by Wickholm et al. (1998). Our deuteration data are consistent with several variants of this model.

A limiting factor in the interpretation of the spin-diffusion experiments is the assignment of the NMR signals, especially in the β-glycan C-4 region, to the polymers of the wood cell wall. The most detailed published assignments are those of Larsson and co-workers (Larsson et al. 1997; Wickholm et al. 1998; Larsson et al. 1999), who deconvoluted the 80–90-ppm region of the ^{13}C spectrum into Gaussian and Lorentzian components assigned to crystalline, paracrystalline and non-crystalline cellulose chains and hemicelluloses. In the wood pulp and textile cellulose spectra that these authors examined, it was possible to separate the signals around 84 ppm from C-4 of non-crystalline cellulose into two closely spaced narrow peaks and one very broad underlying peak. The broad C-4 peak was assigned to cellulose surfaces within aggregates, fitting against one another in disordered ways. The two narrow peaks were assigned to the surfaces of microfibrils exposed at the surface of aggregates.

On the other hand, Newman and Hemmingson (1995), Newman (1999) and Newman and Davidson (2004) assigned the C-4 region of the spectra without separating it into broad and narrow signals. These different interpretations of the spectra do not affect the calculation of lateral microfibril dimensions from the intensity ratio of the C-4 signal of surface and interior chains, which are agreed to lie below and above 86 ppm, respectively (Newman 1999; Larsson et al. 1999), but they lead to different ideas of the level of order present in native cellulose (Viëtor et al. 2002). Dissection of this spectral region, where chemical shifts are highly dependent on conformation, is particularly difficult. Gaussian or Lorentzian fitting is required for statistical deconvolution (Wickholm et al. 2001), but from what is known about the relationship of chemical shift to conformation (Jarvis 1994; Newman and Davidson 2004) there is no *a priori* reason to expect that peak shapes will be Gaussian, Lorentzian, or even unimodal and symmetrical.

A further consequence of the uncertainty in interpretation of the 84-ppm region of the NMR spectrum concerns the shoulder commonly observed at approximately 82 ppm. Newman (1999) assigned this signal, in a spectrum from eucalyptus kraft pulp, to C-4 of xylans conformationally aligned with cellulose. Larsson et al. (1999) included much of the signal intensity in this region to the upfield wing of the broad band for surface cellulose within aggregates, although xylans were also considered to contribute to this broad band and a small, separate, narrow signal at 82 ppm was assigned to C-4 of xylan in hardwood (Wickholm et al. 1998, Teleman et al. 2001) and either xylan or glucomannan in softwood pulp (Hult et al. 2000).

Our observations of spin diffusion in the 82-ppm region of the Sitka spruce spectra can be interpreted in two ways, depending on the signal assignments. If surface cellulose chains within aggregates make a major contribution to the intensity in this region (Larsson et al. 1999), their contribution to the spin mixing curves would be expected to resemble the spin mixing curve for the 84-ppm signal. The additional contribution from hemicelluloses would then have to be very different, resembling the spin mixing curve for the 80-ppm signal. The alternative interpretation is that the 82-ppm signal intensity is derived mainly from hemicelluloses (Newman 1999), but that these are located in closer association with cellulose than are the hemicelluloses giving rise to the 80-ppm signal. The convergence of the 82-ppm and acetyl signals suggests that the polymers concerned include acetylated glucomannans, although the possibility that C-4 signals from xylans were also represented in this spectral region cannot be excluded. It might be expected that acetylated hemicelluloses would be unable to bind to cellulose and might therefore be in closer proximity to lignin, but the spin-diffusion data indicate that the polysaccharides most closely associated with lignin were those with C-4 signals near 80 ppm, and there was no evidence that these were acetylated.

Some of the hemicelluloses with C-4 at 82 ppm may have been associated with the substantial fraction of the hemicellulose C-1 signal hidden at approximately 104 ppm beneath the cellulose C-1 region, which must have had rather similar spin-diffusion characteristics, because it perturbed the cellulose signal only to a small extent. The relationship between the 102-ppm C-1 peak and the 80-ppm C-4 peak was not clear, although both were derived from relatively mobile hemicelluloses. We could not determine whether these signals represented xylans, glucomannans, or a mixture of the two, a problem encountered by others (Maunu 2002 and references cited therein). No signal exclusively attributable to xylans appears to have been identified so far in the ^{13}C NMR spectra of softwoods.

By adjusting the values of the spin-diffusion coefficient and spin-lattice relaxation time associated with each type of polymer, it was possible to match the main features of the observed spin-diffusion curves, although detailed statistical fitting was not attempted (Figure 9). The spin-diffusion coefficients required to match the experimental observations (Table 2) were an order of magnitude lower than those calculated from the measured effective ^1H T_2 values, as previously observed for primary cell walls (Ha et al. 1998). The discrepancy is attributed to anisotropy in proton spin diffusion. In other words, ^1H T_2 relaxation is dominated by spin-spin interactions along the length

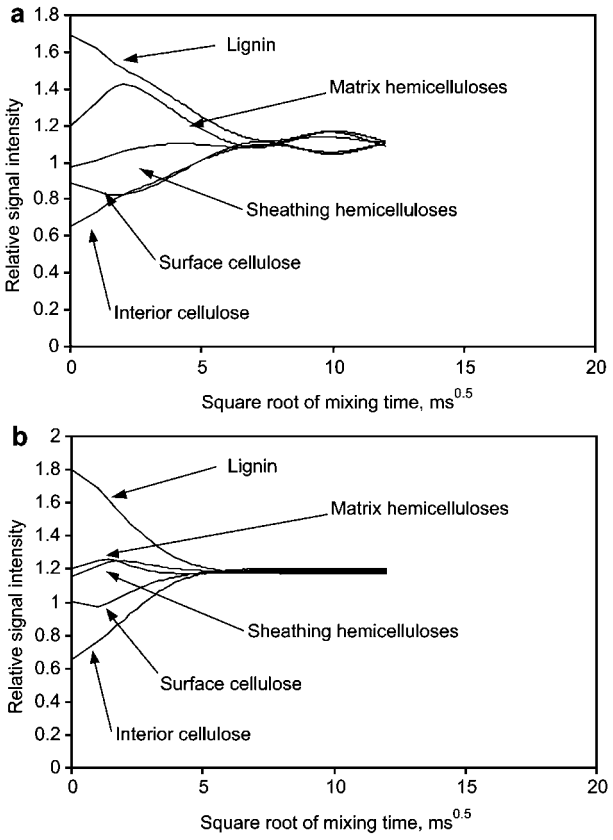

Figure 9 Simulated spin-diffusion curves for model systems, with parameters summarised in Table 2. (a) Simulation for the model system shown in Figure 2, with aggregated microfibrils. Oscillation at long mixing times is an artefact. (b) Simulation for a model system comprising a single microfibril with concentric sheaths of hemicellulose and a lignin-hemicellulose matrix.

Table 2 Fitted values of the proton spin diffusion coefficient K_d and proton spin-lattice relaxation time ^1H T_1 used to generate the simulated spin-diffusion curves in Figure 9.

	K_d (nm^2 ms^{-1})	^1H T_1 (ms)
Lignin	0.06	300
Hemicellulose sheath	0.08	400
Surface cellulose	0.09	500
Interior cellulose	0.1	10000
Matrix hemicellulose	0.08	300

of each polymer, in which direction the relatively rigid C–H protons are closely spaced. Radial spin diffusion, on the other hand, must cross the hydrogen-bonded interfaces between polymer chains, where, in the presence of water, there is more thermal motion to interfere with ^1H spin-spin interactions. The values of the spin-lattice relaxation time ^1H T_1 were allowed to vary from one polymer to another much more widely than those observed, since the observed values were averaged by spin diffusion. Allowing for residual effects of ^1H T_1 relaxation was recommended by Kenwright and Packer (1990), although they did not suggest a way in which it might be achieved.

Similar modelling of a single cellulose microfibril surrounded by a lignin-hemicellulose matrix did not yield simulated spin-diffusion curves consistent with the experimental observations, but predicted that spin equilibration between all components occurred simultaneously (Figure 9). A model in which the 16 microfibrils shown in Figure 1 were consolidated into an array without the interstitial hemicellulose, which was removed to the outer face of the array, gave simulated spin-diffusion curves very similar to those shown in Figure 9 (data not shown) when the input parameters were the same. The two models with aggregated microfibrils are therefore not distinguishable on the basis of our spin-diffusion observations. It is likely that the observed data could be matched by other detailed modifications of these models.

From the spin diffusion and FTIR data it is possible to reach a number of qualitative conclusions on the nanostructure of Sitka spruce. First, lignin and cellulose were separated by distances significantly greater than the distances separating the surface and interior chains of cellulose microfibrils. This conclusion is consistent with the models of Fahlén and Salmén (2005), Hafren et al. (1999) and Terashima et al. (2004), in which lignin is located in the matrix surrounding aggregates of microfibrils. Second, water penetrated into these aggregates only partially or not at all. Third, hemicelluloses showed a range of spin-diffusion behaviour consistent with the presence of separate hemicellulose pools associated with lignin and associated with cellulose. It has been suggested (Akerholm and Salmén 2004) that glucomannans are in close mechanical association with softwood cellulose, while xylans are associated with lignin. We found that the hemicelluloses showing clearest evidence of association with lignin did not seem to be acetylated, but had C-4 signals at approximately 80 ppm, whereas published assignments of xylan C-4 signals are centred on 84 ppm (Wickholm et al. 1998). Chemical shift differences of this

order between disordered and ordered xylan chains are quite feasible (Jarvis 1994). Because of the sensitivity of the hemicellulosic C-4 signals to conformation, there is too much uncertainty about the assignments. Thus, spin-diffusion data alone cannot be used to determine whether the hemicelluloses associated with lignin are glucommannans, xylans or a mixture of the two.

Acknowledgements

We thank S. Mochan and B. Gardiner of the Northern Research Station, Forest Research for the provision of timber, P. McLean for cutting discs, and SHEFC and EPSRC for financial support.

References

Ahvazi, B.C., Argyropoulos, D.S. (1999) Proton spin-lattice relaxation time measurements of solid wood and its constituents as a function of pH: Part II. Solid State Nucl. Magn. Reson. 15:49–57.

Akerholm, M., Salmén, L. (2004) Softening of wood polymers induced by moisture studied by dynamic FTIR spectroscopy. J. Appl. Polym. Sci. 94:2032–2040.

Bardet, M., Gagnaire, D., Nardin, R., Robert, D., Vincendon, M. (1986) Use of C-13 enriched wood for structural NMR investigation of wood and wood components, cellulose and lignin, in solid and in solution. Holzforschung 40:17–24.

Bertaud, F., Holmbom, B. (2004) Chemical composition of earlywood and latewood in Norway spruce heartwood, sapwood and transition zone wood. Wood Sci. Technol. 38:245–256.

Fahlén, J., Salmén, L. (2005) Pore and matrix distribution in the fiber wall revealed by atomic force microscopy and image analysis. Biomacromolecules 6:433–438.

Ha, M.A., Evans, B.W., Jarvis, M.C., Apperley, D.C., Kenwright, A.M. (1996) CP-MAS NMR of highly mobile hydrated biopolymers: polysaccharides of *Allium* cell walls. Carbohydr. Res. 288:15–23.

Ha, M.A., Apperley, D.C., Evans, B.W., Huxham, I.M., Jardine, W.G., Viëtor, R.J., Reis, D., Vian, B., Jarvis, M.C. (1998) Fine structure in cellulose microfibrils: NMR evidence from onion and quince. Plant J. 16:183–190.

Hafren, J., Fujino, T., Itoh, T. (1999) Changes in cell wall architecture of differentiating tracheids of *Pinus thunbergii* during lignification. Plant Cell Physiol. 40:532–541.

Haw, J.F., Maciel, G.E., Schroeder, H.A. (1984) Carbon-13 nuclear magnetic resonance spectrometric study of wood and wood pulping with cross polarization and magic-angle spinning. Anal. Chem. 56:1323–1329.

Hult, E.L., Larsson, P.T., Iversen, T. (2000) A comparative CP/MAS C-13-NMR study of cellulose structure in spruce wood and kraft pulp. Cellulose 7:35–55.

Jarvis, M.C. (1994) Relationship of chemical shift to glycosidic conformation in the solid-state ^{13}C NMR spectra of (1→4)-linked glucose polymers and oligomers: Anomeric and related effects. Carbohydr. Res. 259:311–318.

Kenwright, A.M., Packer, K.J. (1990) On T_1 cancellation schemes in Goldman-Shen-type experiments. Chem. Phys. Lett. 173: 471–475.

Kim, Y.S., Newman, R.H. (1995) Solid-state C-13 NMR study of wood degraded by the brown-rot fungus *Gloeophyllum trabeum.* Holzforschung 49:109–114.

Larsson, P.T., Wickholm, K., Iversen, T. (1997) A CP/MAS C-13 NMR investigation of molecular ordering in celluloses. Carbohydr. Res. 302:19–25.

Larsson, P.T., Hult, E.L., Wickholm, K., Pettersson, E., Iversen, T. (1999) CP/MAS C-13-NMR spectroscopy applied to structure and interaction studies on cellulose I. Solid State Nucl. Magn. Reson. 15:31–40.

Liitia, T., Maunu, S.L., Hortling, B. (2000) Solid-state NMR studies of residual lignin and its association with carbohydrates. J. Pulp Paper Sci. 26:323–330.

Maunu, S.L. (2002) NMR studies of wood and wood products. Prog. Nucl. Magn. Reson. Spectrosc. 40:151–174.

Newman, R.H. (1992) Nuclear magnetic resonance study of spatial relationships between chemical components in wood cell walls. Holzforschung 46:205–210.

Newman, R.H. (1999) Estimation of the lateral dimensions of cellulose crystallites using C-13 NMR signal strengths. Solid State Nucl. Magn. Reson. 15:21–29.

Newman, R.H., Davidson, T.C. (2004) Molecular conformations at the cellulose-water interface. Cellulose 11:23–32.

Newman, R.H., Hemmingson, J.A. (1990) Determination of the degree of cellulose crystallinity in wood by C-13 nuclear magnetic resonance spectroscopy. Holzforschung 44:351–355.

Newman, R.H., Hemmingson, J.A. (1995) C-13 NMR distinction between categories of molecular order and disorder in cellulose. Cellulose 2:95–110.

Singh, A., Daniel, G., Nilsson, T. (2002) Ultrastructure of the S-2 layer in relation to lignin distribution in *Pinus radiata* tracheids. J. Wood Sci. 48:95–98.

Sivonen, H., Nuopponen, M., Maunu, S.L., Sundholm, F., Vuorinen, T. (2003) Carbon-13 cross-polarization magic angle spinning nuclear magnetic resonance and Fourier transform infrared studies of thermally modified wood exposed to brown and soft rot fungi. Appl. Spectrosc. 57:266–273.

Tekely, P., Vignon, M.R. (1987a) Cross polarization magic angle spinning C-13 NMR characterization of steam exploded poplar wood. J. Wood Chem. Technol. 7:215–228.

Tekely, P., Vignon, M.R. (1987b) Proton T_1 and T_2 relaxation times of wood components using C-13 CP MAS NMR. J. Polym. Sci. C-Polym. Lett. 25:257–261.

Teleman, A., Larsson, P.T., Iversen, T. (2001) On the accessibility and structure of xylan in birch kraft pulp. Cellulose 8:209–215.

Terashima, N., Awano, T., Takabe, K., Yoshida, M. (2004) Formation of macromolecular lignin in ginkgo xylem cell walls as observed by field emission scanning electron microscopy. C. R. Biol. 327:903–910.

Viëtor, R.J., Newman, R.H., Ha, M.A., Apperley, D.C., Jarvis, M.C. (2002) Conformational features of crystal-surface cellulose from higher plants. Plant J. 30:721–731.

Wickholm, K., Larsson P.T., Iversen, T. (1998) Assignment of non-crystalline forms in cellulose I by CP/MAS C-13 NMR spectroscopy. Carbohydr. Res. 312:123–129.

Wickholm, K., Hult, E.L., Larsson, P.T., Iversen, T., Lennholm, H. (2001) Quantification of cellulose forms in complex cellulose materials: A chemometric model. Cellulose 8:139–148.

Wikberg, H., Maunu, S.L. (2004) Characterisation of thermally modified hard- and softwoods by C-13 CPMAS NMR. Carbohydr. Polym. 58:461–466.

Zhang, S., Mehring, M. (1989) A modified Goldman-Shen NMR pulse sequence. Chem. Phys. Lett. 160:644.

Received March 13, 2006. Accepted August 2, 2006.